

The chaotic behavior of the Bianchi IX model under the influence of quantum effects

Martin Bojowald¹, David Brizuela², Paula Calizaya Cabrera³, and Sara F. Uria²

¹*Institute for Gravitation and the Cosmos, The Pennsylvania State University, 104 Davey Lab, University Park, PA 16802, USA*

²*Department of Physics and EHU Quantum Center, University of the Basque Country UPV/EHU, Barrio Sarriena s/n, 48940 Leioa, Spain*

³*Department of Physics and Astronomy, Louisiana State University, Baton Rouge, LA 70803, USA*

Abstract

A quantum analysis of the vacuum Bianchi IX model is performed, focusing in particular on the chaotic nature of the system. The framework constructed here is general enough for the results to apply in the context of any theory of quantum gravity, since it includes only minimal approximations that make it possible to encode the information of all quantum degrees of freedom in the fluctuations of the usual anisotropy parameters. These fluctuations are described as canonical variables that extend the classical phase space. In this way, standard methods for dynamical systems can be applied to study the chaos of the model. Two specific methods are applied that are suitable for time-reparameterization invariant systems. First, a generalized version of the Misner-Chitre variables is constructed, which provides an isomorphism between the quantum Bianchi IX dynamics and the geodesic flow on a suitable Riemannian manifold, extending, in this way, the usual billiard picture. Secondly, the fractal dimension of the boundary between points with different outcomes in the space of initial data is numerically analyzed. While the quantum system remains chaotic, the main conclusion is that its strength is considerably diminished by quantum effects as compared to its classical counterpart.

1 Introduction

According to the Belinski-Khalatnikov-Lifshitz (BKL) conjecture [1] the dynamics of the spacetime near a generic spacelike singularity becomes local (in the sense that different spatial points decouple), oscillatory, and dominated by pure gravity. Therefore, the vacuum Bianchi IX (also known as Mixmaster) model [2, 3] is assumed to provide a proper characterization of the evolution of each of these points. A formal proof of the BKL conjecture is not yet available, but it is supported by a large number of numerical studies [4–6]. Therefore, the general working assumption is that this conjecture is true, and thus the study of the Mixmaster model has received much attention. In particular, regarding its specific properties, there is a wide literature on the chaotic nature of the Mixmaster—and hence the BKL—dynamics. In fact, in the context of chaos, this is one of the most discussed solutions of the Einstein equations [7, 8]. However, due to the nature of general relativity, usual dynamical methods to study chaos cannot be applied, as they are not covariant (observer independent). Hence, different techniques have been proposed and implemented to prove the chaotic nature of the Mixmaster model.

The first attempts in this direction were already made by the original authors of the BKL conjecture [1]. Specifically, they showed that, under certain assumptions, the full dynamics of the system given by the Einstein equations can be approximated by a discrete map. A large number of iterations of this map corresponds thus to the asymptotic limit of the evolution towards the singularity. They were then able to prove that the dependence on the initial conditions vanished in such a limit. A few years later, making use of this same discrete map, but considering the topological and metric entropies of its related one-dimensional Poincaré section, similar conclusions were found in Refs. [9–11]. Thus, both approaches proved that the discrete dynamics is chaotic, though the full dynamics was still to be analyzed.

Subsequent studies were then devoted to an analysis of the full dynamics, solving numerically the corresponding Einstein equations. Most of them focused on the computation of the Lyapunov exponents, since, in usual dynamical systems, a positive value of any of these exponents characterizes the system to be chaotic. However, in the present context, this led to several (apparent) contradictions: depending on the time parameterization, both positive and nonpositive values were obtained [12–17]. By construction, all these results were obtained in a given coordinate system and were thus observer dependent. Therefore, at the time, the usual explanation of the controversy pointed to a violation of general covariance. However, this was not the case: as Motter later showed [18], the sign of the Lyapunov exponent, if properly defined, is invariant under coordinate

transformations. In fact, another important conclusion of this work was that none of the mentioned investigations satisfied the requirements for a proper definition of the Lyapunov exponent. More precisely, in order to have an invariant meaning, the computation of this exponent must be done in certain set of coordinates, so that the system meets some specific conditions [18]. Hence, one of these suitable coordinate systems was chosen in [19] and, just by an analytical computation of the exponent, it was confirmed that the full Mixmaster dynamics is indeed chaotic. More specifically, it was proven that it is isomorphic to a billiard on the two-dimensional Lobachevsky plane, which is well known to exhibit chaos, as it has convex and therefore defocusing walls [20].

On the other hand, another completely different approach was followed to test the chaotic nature of the Mixmaster dynamics, by means of observer independent—and therefore covariant—fractal methods [21, 22]. These studies considered both the discrete map, as well as the full dynamics, and showed that this system is characterized by the presence of a strange repeller with fractal dimensions, which ensures chaos. Moreover, the authors of Ref. [21] were able to quantify chaos by computing different relevant quantities, such as the uncertainty exponent or the multifractal dimensions of the repeller.

However, even if it is now generally accepted that the classical Mixmaster dynamics is chaotic, quantum effects are expected to be relevant asymptotically, and they might completely modify the classical picture in the extreme regimes close to the spacelike singularity. Several analyses can be found in the literature, proposing different quantizations of this model, and focused on a variety of questions, such as the avoidance of the singularity, or the modifications of its oscillatory dynamics (see, e.g., Refs. [23–38]). In particular, some works have been devoted to analyzing the survival of chaos, but so far with mixed results [39–42]. In these approaches specific properties that may reduce chaos have been identified (such as, for instance, an isotropization of the system, or a possible bounded curvature), but none of them has studied these effects in a general way, such that it can be applied to any quantum-gravity model.

Therefore, in the present paper, we present a systematic semiclassical analysis that will allow us to study how quantum effects modify the chaotic behavior of the Mixmaster model. Our framework is based on a decomposition of the wave function into its infinite set of moments, and we will introduce certain assumptions (a Gaussian-like state and small fluctuations) so that quantum effects will be encoded in a finite set of canonical variables. In this way, the system can be described in a phase space, which constitutes an extension of the classical phase space by the fluctuation degrees of freedom, and thus usual dynamical-systems techniques can be applied to study chaos. In particular, the two methods mentioned above (the computation of the covariant Lyapunov exponent and fractal methods) will be applied to this quantum system. Our main conclusion will be that, even if the quantum system is still chaotic, quantum effects significantly reduce the level of chaos.

The paper is organized as follows. In Sec. 2 the classical Mixmaster model is presented. Sec. 3 describes the construction of the framework that will describe the Mixmaster dynamics in a semiclassical regime. Sec. 4 contains a qualitative description of this dynamics. In Sec. 5 the chaotic nature of the model is studied following two different approaches. More precisely, in Sec. 5.1 the covariant Lyapunov exponent is computed, while in Sec. 5.2 the fractal dimension of the repeller set in the space of initial data is analyzed. Finally, in Sec. 6 the main results of the paper are discussed and summarized.

2 Classical model

The vacuum Bianchi IX model, also known as the Mixmaster model, is described by the metric

$$ds^2 = -N^2 dt^2 + \sum_{i=1}^3 a_i^2 \sigma_i^2, \quad (1)$$

where N is the lapse function, a_i are the expansion rates for each of the three space directions, and σ_i are 1-forms on the three sphere that satisfy $d\sigma_i = \frac{1}{2}\epsilon_{ijk}\sigma_j \wedge \sigma_k$. A particular parameterization of these forms can be given in terms of the Euler angles,

$$\begin{aligned} \sigma_1 &:= \sin \psi d\theta - \cos \psi \sin \theta d\phi, \\ \sigma_2 &:= \cos \psi d\theta + \sin \psi \sin \theta d\phi, \\ \sigma_3 &:= -d\psi - \cos \theta d\phi. \end{aligned} \quad (2)$$

As first pointed out by Misner [3], it is convenient to define basic variables that, instead of describing the change of every individual spatial direction, determine the change of the volume and shape of the three-dimensional

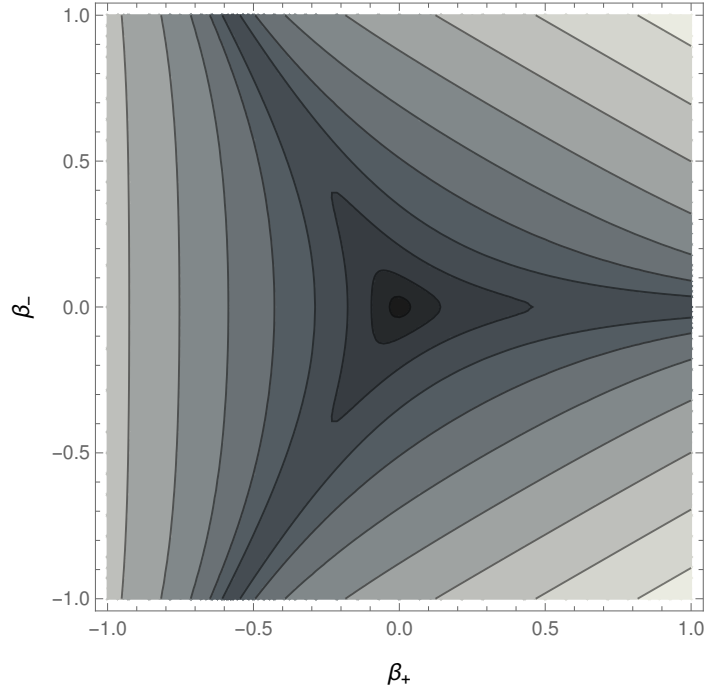


Figure 1: Contour plot of the classical Bianchi IX potential $V(\beta_+, \beta_-)$ given by Eq. (6).

geometry. More precisely, one can perform a change of variables from the three expansion rates a_i to a new set of variables given by α , defined as

$$e^\alpha = (a_1 a_2 a_3)^{1/3}, \quad (3)$$

encoding the volume of the spatial sections, and the two shape parameters β_+ and β_- , defined as the logarithmic rates

$$\begin{aligned} \beta_+ &:= -\frac{1}{2} \ln \left[\frac{a_3}{(a_1 a_2 a_3)^{1/3}} \right], \\ \beta_- &:= \frac{1}{2\sqrt{3}} \ln \left(\frac{a_1}{a_2} \right), \end{aligned} \quad (4)$$

as a description of the anisotropy.

In terms of these so-called Misner variables, the Hamiltonian constraint for the Mixmaster model reads

$$\mathcal{C} = \frac{1}{2} e^{-3\alpha} (-p_\alpha^2 + p_-^2 + p_+^2) + e^\alpha V(\beta_+, \beta_-) = 0. \quad (5)$$

This constraint equation requires an energy balance between the potential

$$V(\beta_+, \beta_-) := \frac{1}{6} \left[e^{-8\beta_+} + 2e^{4\beta_+} \left(\cosh(4\sqrt{3}\beta_-) - 1 \right) - 4e^{-2\beta_+} \cosh(2\sqrt{3}\beta_-) \right], \quad (6)$$

whose contour plot is shown in Fig. 1, and the kinetic term, which is a quadratic combination of the momenta $p_\alpha := -(e^{3\alpha}/N)d\alpha/dt$ and $p_\pm := (e^{3\alpha}/N)d\beta_\pm/dt$.

The dynamics of this model describes an expanding (or contracting) universe. Therefore the volume, and thus the variable α , are monotonic functions of coordinate time, which allows us to define α as the internal time variable by imposing the gauge $\alpha = t$. The deparameterization of the above constraint then leads to the physical (generically nonvanishing) Hamiltonian,

$$H := -p_\alpha = [p_+^2 + p_-^2 + 2e^{4\alpha} V(\beta_+, \beta_-)]^{1/2}. \quad (7)$$

In this gauge, the independent dynamical variables are the shape parameters β_\pm along with their momenta p_\pm .

Their equations of motion are obtained by computing their Poisson brackets with the Hamiltonian,

$$\dot{\beta}_+ = \{\beta_+, H\} = \frac{p_+}{H}, \quad (8)$$

$$\dot{\beta}_- = \{\beta_-, H\} = \frac{p_-}{H}, \quad (9)$$

$$\dot{p}_+ = \{p_+, H\} = -\frac{e^{4\alpha}}{H} \frac{\partial V(\beta_+, \beta_-)}{\partial \beta_+}, \quad (10)$$

$$\dot{p}_- = \{p_-, H\} = -\frac{e^{4\alpha}}{H} \frac{\partial V(\beta_+, \beta_-)}{\partial \beta_-}, \quad (11)$$

where the dot stands for a derivative with respect to α .

3 Quantum model

We will perform a canonical quantization of the system by promoting the classical Hamiltonian (7) to a quantum operator \hat{H} , which will define the dynamics of the wave function by the usual Schrödinger equation $\hat{H}\Psi = i\hbar\partial\Psi/\partial\alpha$. However, instead of analyzing the evolution of the wave function, we will directly study the dynamics of the central moments,

$$\Delta(\beta_+^i \beta_-^j p_+^k p_-^l) := \langle (\hat{\beta}_+ - \beta_+)^i (\hat{\beta}_- - \beta_-)^j (\hat{p}_+ - p_+)^k (\hat{p}_- - p_-)^l \rangle_{\text{Weyl}}, \quad (12)$$

where the subscript Weyl implies a completely symmetric ordering of the basic operators, the indices i, j, k , and l are nonnegative integers, and, from this point on, we define $\beta_+ := \langle \hat{\beta}_+ \rangle$, $\beta_- := \langle \hat{\beta}_- \rangle$, $p_+ := \langle \hat{p}_+ \rangle$, and $p_- := \langle \hat{p}_- \rangle$. For such a purpose, following the framework presented in [43], one needs to define an effective Hamiltonian H_Q as the expectation value of the Hamiltonian operator $H_Q := \langle \hat{H} \rangle$. By performing a formal series expansion, H_Q can be written in terms of the expectation values of the basic variables, $\langle \beta_+ \rangle$, $\langle \beta_- \rangle$, $\langle p_+ \rangle$, $\langle p_- \rangle$, and the central moments defined above. The time derivative of each of these variables is then given by its Poisson bracket with the effective Hamiltonian H_Q , which can be computed making use of the definition

$$\{\langle \hat{X} \rangle, \langle \hat{Y} \rangle\} = \frac{1}{i\hbar} \langle [\hat{X}, \hat{Y}] \rangle \quad (13)$$

for any two operators \hat{X} and \hat{Y} , and extended to products of expectation values by using the Leibniz rule. Explicit formulas for the Poisson brackets of moments can be found in [43, 44].

In this way, instead of dealing with a partial differential equation for the wave function, one needs to solve a system of ordinary differential equations. Both types of differential equations describe the very same dynamics and solving ordinary differential equations is usually an easier task. However, in the present case it does pose a challenge as the infinitely many moments (12) are evolved by a large number of equations that in general are strongly coupled for nonquadratic Hamiltonians. For practical applications, some approximation is therefore necessary in order to deal with this system. A standard approach is to introduce a truncation by neglecting all moments higher than a certain order, which leads to a finite system that can be solved numerically. In this context the order of a given moment (12) is defined as the sum of its indices $i + j + k + l$. However, in the present paper, we will follow another approach by imposing two different assumptions, spelled out in the next subsection. Instead of truncating the infinite tower of moments by setting infinitely many moments equal to zero, the new assumptions implement a closure condition that maintains nonvanishing higher moments but assumes suitable expressions for them in a finite-dimensional parameterization. The specific closure assumption will allow us to obtain an exact summation of the infinite series that defines the effective Hamiltonian H_Q , in such a way that we will be able to work with an extended though finite-dimensional phase space.

3.1 Closure conditions

Our first approximation concerns the definition of the effective Hamiltonian H_Q . As mentioned above, this expression is defined as the expectation value of the Hamiltonian operator \hat{H} , such that its Hamilton's equation with the Poisson bracket (13) are equivalent to the evolution of moments of a state following the Schrödinger dynamics. The resulting H_Q therefore depends on the ordering chosen for the operator \hat{H} . For instance, if \hat{H} is Weyl-ordered, the corresponding H_Q directly depends on the moments defined with the same

ordering through a Taylor expansion, and there are no additional terms with an explicit dependence on \hbar from re-ordering products.

In the present case, it is more convenient to assume that \hat{H}^2 is Weyl-ordered and to define the quantum Hamiltonian as $H_Q := \sqrt{\langle \hat{H}^2 \rangle}$, an assumption that can also be motivated by first quantizing the constraint (5) and then deparameterizing after quantization. The evolution generated by H_Q does not exactly correspond to the Schrödinger evolution generated by \hat{H} . However, these two possible definitions differ only by a fluctuation term because we have the exact relation

$$\langle \hat{H}^2 \rangle = \langle \hat{H} \rangle^2 + \langle (\hat{H} - \langle \hat{H} \rangle)^2 \rangle. \quad (14)$$

Therefore, as long as the relative fluctuations $\langle (\hat{H} - \langle \hat{H} \rangle)^2 \rangle / H^2$ are small, the effective dynamics given by H_Q will accurately describe the Schrödinger flow of states.

The main reason to perform this approximation is that it implies a greatly simplified expression for the effective Hamiltonian in terms of the moments. More precisely, performing an expansion around the expectation values of the basic operators, the square of the effective Hamiltonian reads

$$\begin{aligned} H_Q^2 &= \langle \hat{H}^2(\hat{\beta}_+, \hat{\beta}_-, \hat{p}_+, \hat{p}_-) \rangle = \sum_{i,j,k,l=0}^{\infty} \frac{1}{i!j!k!l!} \frac{\partial^{i+j+k+l} H^2(\beta_+, \beta_-, p_+, p_-)}{\partial \beta_+^i \partial \beta_-^j \partial p_+^k \partial p_-^l} \Delta(\beta_+^i \beta_-^j p_+^k p_-^l) \\ &= p_+^2 + \Delta(p_+^2) + p_-^2 + \Delta(p_-^2) + e^{4\alpha} \sum_{i,j=0}^{\infty} \frac{1}{i!j!} \frac{\partial^{i+j} V(\beta_+, \beta_-)}{\partial \beta_+^i \partial \beta_-^j} \Delta(\beta_+^i \beta_-^j), \end{aligned} \quad (15)$$

where, as already mentioned, we have defined \hat{H}^2 to be Weyl-ordered. Note that H is the classical Hamiltonian and, in the last equality, its precise form (7) has been taken into account. In particular, since H^2 is quadratic in the momenta p_{\pm} , only their fluctuations appear in this effective Hamiltonian, and higher-order moments only depend on the shape parameters. One can already see at this point that the structure of this effective Hamiltonian is quite similar to the classical one: it has a kinetic part, which is, in some sense, quadratic in momentum variables, and a potential term, that, up to the global factor $e^{4\alpha}$, only depends on the position variables. We will make this structure more explicit below.

At this point one could obtain the equations of motion for the expectation values of basic operators and the moments by computing their Poisson brackets with H_Q . However, the equations are very complicated, in particular because the moments do not have canonical brackets with one another. Nevertheless, according to Darboux' theorem, and its extension to nonsymplectic manifolds, any Poisson manifold can be described locally by canonical coordinates, given by generalized positions and momenta, as well as Casimir variables. For instance, for fluctuations and correlations one can define the following change of variables [45–49],

$$\begin{aligned} \Delta(p_+^2) &= p_{s_1}^2 + \frac{U_1}{s_1^2}, & \Delta(\beta_+^2) &= s_1^2, \\ \Delta(p_-^2) &= p_{s_2}^2 + \frac{U_2}{s_2^2}, & \Delta(\beta_-^2) &= s_2^2, \\ \Delta(\beta_+ p_+) &= s_1 p_{s_1}, & \Delta(\beta_- p_-) &= s_2 p_{s_2}, \end{aligned} \quad (16)$$

ignoring cross-correlations between the two pairs of degrees of freedom. From these definitions, we note that only the sign of either s_i or p_{s_i} has physical meaning: both (s_i, p_{s_i}) and $(-s_i, -p_{s_i})$ represent the same physical state. Thus, we will choose s_i to be positive definite (since it parameterizes the fluctuation of β_{\pm} , it cannot be vanishing), and let p_{s_i} be defined on the whole real line. Under a second-order truncation (neglecting all moments of an order three and higher), s_i and p_{s_i} are canonically conjugate, satisfying $\{s_i, p_{s_j}\} = \delta_{ij}$, for $i, j = 1, 2$, while U_i are Casimir variables that have vanishing Poisson brackets with the different variables. These encode the information about the Heisenberg uncertainty relation, since they obey

$$\begin{aligned} \Delta(\beta_+^2) \Delta(p_+^2) - \Delta(\beta_+ p_+)^2 &= U_1 \geq \frac{\hbar^2}{4}, \\ \Delta(\beta_-^2) \Delta(p_-^2) - \Delta(\beta_- p_-)^2 &= U_2 \geq \frac{\hbar^2}{4}. \end{aligned} \quad (17)$$

For higher-order moments, the corresponding canonical variables are hard to find explicitly, and their expressions are usually lengthy in cases in which they are known (see Ref. [49] for a fourth-order derivation

for a single pair of classical degrees of freedom, as well as a second-order mapping for two pairs of degrees of freedom with cross-correlations). Since $\Delta(\beta_+^i \beta_-^j)$ are the only higher-order moments that appear in the effective Hamiltonian (15), the second approximation we will perform here is to parameterize these higher-order moments solely in terms of the s_i defined above. In order to choose a meaningful parameterization, we base our choice in the form of the moments for a Gaussian state and impose

$$\Delta(\beta_+^{2n} \beta_-^{2m}) = \frac{s_1^{2n} s_2^{2m} (2n)!(2m)!}{2^n 2^m n!m!} \quad (18)$$

for nonnegative integers n, m , while $\Delta(\beta_+^i \beta_-^j) = 0$ otherwise. With this second approximation we are thus assuming that the moments corresponding to the shape parameters keep the Gaussian form all along the evolution, an assumption that can be considered valid in a semiclassical context. More precisely, since, as will be explained in Sec. 4, the classical dynamics follows periods of free evolution separated from one another by quick reflections on steep potential walls, a semiclassical state can be expected to maintain nearly Gaussian form for a considerable amount of time. In particular, the state is not expected to split up into separate wave packets and develop multimodality, as it would happen for instance in tunneling situations. Our assumptions are therefore justified and they may be tested further by including higher-order terms in the Hamiltonian, which we leave for future work.

3.2 Summation

Replacing now the form of the moments (18) in the effective Hamiltonian (14), it is possible to perform exactly the infinite sum. In this way, we obtain the following closed form for the effective Hamiltonian,

$$H_Q^2 = \langle \hat{H}^2 \rangle = p_+^2 + p_-^2 + p_{s_1}^2 + p_{s_2}^2 + \frac{U_1}{s_1^2} + \frac{U_2}{s_2^2} + 2e^{4\alpha} V_Q(\beta_+, \beta_-, s_1, s_2), \quad (19)$$

with the corresponding effective potential defined as

$$V_Q(\beta_+, \beta_-, s_1, s_2) := \frac{1}{6} \left[e^{-8\beta_+ + 32s_1^2} + 2e^{4\beta_+ + 8s_1^2} \left(e^{24s_2^2} \cosh(4\sqrt{3}\beta_-) - 1 \right) - 4e^{-2\beta_+ + 2s_1^2 + 6s_2^2} \cosh(2\sqrt{3}\beta_-) \right]. \quad (20)$$

Hence, the only relevant variables of our quantum model will be β_{\pm} , p_{\pm} , s_i , p_{s_i} , and U_i with $i = 1, 2$. In fact, the variables U_i are constants of motion. In the Hamiltonian they appear as centrifugal potential terms and thus can be regarded as an angular momentum that prevents the position variables s_i from reaching the origin, enforcing, in this way, the uncertainty relation. The Hamiltonian has now a clear structure of a kinetic part, quadratic in momenta, plus a potential term, which, up to the global factor $e^{4\alpha}$, only depends on position variables. The classical phase space, given by the two couples (β_{\pm}, p_{\pm}) , is thus enlarged by the two new degrees of freedom described by (s_i, p_{s_i}) and by the parameters U_i , which encode the quantum effects. The vanishing of these quantum variables leads to the classical limit, as can be easily seen by comparing (19) with its classical counterpart (7).

The equations of motion for the different variables read

$$\dot{\beta}_{\pm} = \{\beta_{\pm}, H_Q\} = \frac{p_{\pm}}{H_Q}, \quad (21)$$

$$\dot{p}_{\pm} = \{p_{\pm}, H_Q\} = -\frac{e^{4\alpha}}{H_Q} \frac{\partial V_Q}{\partial \beta_{\pm}}, \quad (22)$$

$$\dot{s}_i = \{s_i, H_Q\} = \frac{p_{s_i}}{H_Q}, \quad (23)$$

$$\dot{p}_{s_i} = \{p_{s_i}, H_Q\} = \frac{1}{H_Q} \left(\frac{U_i}{s_i^3} - e^{4\alpha} \frac{\partial V_Q}{\partial s_i} \right), \quad (24)$$

which explicitly shows the back-reaction of the quantum variables (s_i, p_{s_i}, U_i) on the classical evolution.

For later convenience, let us note that the full time-dependent effective potential term that appears in the Hamiltonian above can be rewritten in the following way:

$$2e^{4\alpha} V_Q = \frac{1}{3} (e^{4\alpha E_1} + e^{4\alpha E_2} + e^{4\alpha E_3}) - \frac{2}{3} (e^{4\alpha E_4} + e^{4\alpha E_5} + e^{4\alpha E_6}), \quad (25)$$

where the exponents E_j ($j = 1, 2, 3, 4, 5, 6$) are defined as

$$\begin{aligned}
E_1 &= 1 - \frac{2\beta_+ - 8s_1^2}{\alpha}, & E_4 &= 1 + \frac{\beta_+ + 2s_1^2}{\alpha}, \\
E_2 &= 1 + \frac{\beta_+ + \sqrt{3}\beta_- + 2s_1^2 + 6s_2^2}{\alpha}, & E_5 &= 1 + \frac{\sqrt{3}\beta_- - \beta_+ + s_1^2 + 3s_2^2}{2\alpha}, \\
E_3 &= 1 + \frac{\beta_+ - \sqrt{3}\beta_- + 2s_1^2 + 6s_2^2}{\alpha}, & E_6 &= 1 - \frac{\sqrt{3}\beta_- + \beta_+ - s_1^2 - 3s_2^2}{2\alpha}.
\end{aligned} \tag{26}$$

4 A qualitative description of the dynamics

The dynamics of the classical Mixmaster model is characterized by a succession of Kasner regimes and transitions as the singularity is approached [2,3]. These regimes are defined as being kinetically dominated, in the sense that the potential term can be neglected in the Hamiltonian. Therefore, according to (7), the classical Hamiltonian is approximately given by the expression $H \approx (p_+^2 + p_-^2)^{1/2}$, which corresponds to that of the exact Kasner model, and describes a free motion: the momenta p_+ and p_- remain constant and the shape parameters β_+ and β_- evolve as linear functions in α . In the two-dimensional plane of the shape parameters, the trajectory is thus a straight line. During this evolution, however, at least one of the exponential terms of the potential (6) is growing in time and, from a certain point on, the potential is no longer negligible. The Kasner approximation then ceases to be valid, the system quickly bounces against the exponential walls depicted in Fig. 1, and enters a new Kasner regime. The transition between successive Kasner epochs is described by a well-known map that relates the pre-bounce to post-bounce values of the momenta (p_+, p_-) and of the constants that characterize the Kasner evolution of the shape parameters (β_+, β_-) (see, e.g., Ref. [50]). In fact, as mentioned in the introduction, this discrete map was already used to conclude that the Mixmaster model is chaotic in the early literature about this subject [1,9–11].

The described behavior is realized for a generic choice of initial values. Nevertheless, there are certain specific values of the momenta during a Kasner regime, for which none of the exponential terms of the potential grows in time. The system thus never reaches an exponential wall and follows a Kasner evolution until it reaches the singularity. More precisely, there are three such possible values: $\{p_- < 0, p_+ = -\frac{p_-}{\sqrt{3}}\}$, $\{p_- > 0, p_+ = \frac{p_-}{\sqrt{3}}\}$, and $\{p_- = 0, p_+ \leq 0\}$, which respectively correspond to the system going to infinity in the plane of the shape parameters through one of the three vertices of the triangular shape of Fig. 1. These are sometimes called exits of the system. Given a set of initial data, some of them end up reaching one of these exits, while others follow an infinite succession of Kasner regimes and form the repeller set. This repeller has a fractal structure, which can be used to analyze the chaos of the system, as will be explained below.

Let us now analyze how the described picture is modified by quantum effects. Numerical integration of the semiclassical evolution equations (21)–(24), not too close to the singularity and for relatively small values of the fluctuations, shows an evolution qualitatively similar to the classical one: the system spends most of the time following Kasner regimes, which are interrupted by rapid transitions when it hits the exponential walls. (For a recent analytic study on quantum Kasner transitions with a similar semiclassical model, we refer the reader to Ref. [38]). This can also be seen analytically. More precisely, neglecting the potential (as well as its derivatives) in the equations of motion (21)–(24), one can easily solve the system and obtain the following explicit evolution of the different variables during a Kasner epoch,

$$\begin{aligned}
p_{\pm} &= \text{const.}, \\
\beta_{\pm} &= \frac{p_{\pm}}{P_Q} \alpha + c_{\pm}, \\
s_i &= \sqrt{\frac{U_i}{B_i^2} + \frac{B_i^2}{P_Q^2} (\alpha + A_i)^2}, \\
p_{s_i} &= \frac{B_i^2 (\alpha + A_i)}{\sqrt{U_i P_Q^2 / B_i^2 + B_i^2 (\alpha + A_i)^2}},
\end{aligned} \tag{27}$$

where c_{\pm} , A_i , and B_i ($i = 1, 2$) are six integration constants. (See also Ref. [51] for a discussion of free quantum dynamics in this language.) In particular B_i encode the constant value of the fluctuation of the momenta: $\Delta(p_+^2) = p_{s_1}^2 + U_1/s_1^2 = B_1^2$, and $\Delta(p_-^2) = p_{s_2}^2 + U_2/s_2^2 = B_2^2$. The value of the Hamiltonian

during these Kasner regimes is given by $P_Q := (p_+^2 + p_-^2 + B_1^2 + B_2^2)^{1/2}$; thus, quantum fluctuations increase its value with respect to its classical counterpart $P := (p_+^2 + p_-^2)^{1/2}$. The variables p_\pm and β_\pm evolve as in the classical model, the only difference being that the velocity of the anisotropies $\dot{\beta}_\pm$ is a bit slower, since it inversely depends on P_Q . Towards the singularity, the variables s_i , which encode the fluctuations of the shape parameters, increase, while their momenta p_{s_i} decrease, tending to their asymptotic values $-|B_i|$.

At this point, one can wonder about the fate of the classical exits mentioned above, where the system follows an infinite Kasner regime all the way to the singularity. It is clear from (19) that, for such an exit to exist for the quantum system, all the exponents $\{E_j\}_{j=1}^6$ in (26) must be nonnegative during the whole Kasner evolution given by (27). As a representative example, let us analyze the behavior of the first exponent, E_1 . During a Kasner regime, this exponent evolves as

$$E_1 = \frac{P_Q - 2p_+}{P_Q} - \frac{2c_+}{\alpha} + \frac{8U_1}{B_1^2\alpha} + \frac{8B_1^2(\alpha + A_1)^2}{P_Q^2\alpha}. \quad (28)$$

The first two terms are the only ones that appear in the classical limit: $(P_Q - 2p_+)/P_Q$ is constant, and $-2c_+/\alpha$ vanishes as $\alpha \rightarrow -\infty$. Therefore, under the classical evolution, the sign of $(P_Q - 2p_+)/P_Q$ rules the asymptotic behavior of this exponential term. In particular, if it is negative, it will define the usual ‘‘classical’’ potential wall asymptotically, with an exponential shape $e^{-m^2\alpha}$, which will eventually put an end to the Kasner dynamics. However, if it is vanishing, the system will be following one of the exit trajectories (under the additional condition that all the other exponents E_j are nonnegative). Finally, if it is positive, E_1 will provide a negligible contribution, and another exponential term E_j will dominate and define the exponential wall as $\alpha \rightarrow -\infty$.

Quantum contributions introduce further α -dependence on the exponent E_1 . In particular, the term with U_1 tends to zero as the singularity is approached, and thus it does not change the classical asymptotic picture. However, the last term, $8B_1^2P_Q^{-2}(\alpha + A_1)^2/\alpha$, increases as $\alpha \rightarrow -\infty$ (just like the variance of a free-particle wave function). Since it is determined by quantum fluctuations, this term is initially small in a semiclassical regime. But if the system is on (or close to) a classical exit trajectory and does not bounce before this term becomes relevant, it will eventually dominate in the expression for E_1 . In such a case, this term will effectively define a potential of the form $e^{k^2\alpha^2}$, breaking the Kasner evolution.

In fact, performing the same analysis for the different exponents E_j , there is always a contribution from a term proportional to the relative fluctuation B_i^2/P_Q^2 that implies a negative value for the corresponding exponent E_j as $\alpha \rightarrow -\infty$. More specifically, the Kasner dynamics of the different exponents read as follows,

$$\begin{aligned} E_2 &= \frac{P_Q + p_+ + \sqrt{3}p_-}{P_Q} + \frac{c_+ + \sqrt{3}c_-}{\alpha} + \frac{2U_1}{B_1^2\alpha} + \frac{6U_2}{B_2^2\alpha} + \frac{2B_1^2}{P_Q^2\alpha}(\alpha + A_1)^2 + \frac{6B_2^2}{P_Q^2\alpha}(\alpha + A_2)^2, \\ E_3 &= \frac{P_Q + p_+ - \sqrt{3}p_-}{P_Q} + \frac{c_+ - \sqrt{3}c_-}{\alpha} + \frac{2U_1}{B_1^2\alpha} + \frac{6U_2}{B_2^2\alpha} + \frac{2B_1^2}{P_Q^2\alpha}(\alpha + A_1)^2 + \frac{6B_2^2}{P_Q^2\alpha}(\alpha + A_2)^2, \\ E_4 &= \frac{P_Q + p_+}{P_Q} + \frac{c_+}{\alpha} + \frac{2U_1}{B_1^2\alpha} + \frac{2B_1^2}{P_Q^2\alpha}(\alpha + A_1)^2, \\ E_5 &= \frac{2P_Q - p_+ + \sqrt{3}p_-}{2P_Q} + \frac{\sqrt{3}c_- - c_+}{2\alpha} + \frac{U_1}{2B_1^2\alpha} + \frac{3U_2}{2B_2^2\alpha} + \frac{B_1^2}{2P_Q^2\alpha}(\alpha + A_1)^2 + \frac{3B_2^2}{2P_Q^2\alpha}(\alpha + A_2)^2, \\ E_6 &= \frac{2P_Q - p_+ - \sqrt{3}p_-}{2P_Q} - \frac{\sqrt{3}c_- + c_+}{2\alpha} + \frac{U_1}{2B_1^2\alpha} + \frac{3U_2}{2B_2^2\alpha} + \frac{B_1^2}{2P_Q^2\alpha}(\alpha + A_1)^2 + \frac{3B_2^2}{2P_Q^2\alpha}(\alpha + A_2)^2. \end{aligned} \quad (29)$$

Therefore, and contrary to the classical case, there is no combination of parameters that would lead to all E_j being simultaneously nonnegative as $\alpha \rightarrow -\infty$. All the classical exits are thus closed by quantum fluctuations.

We will now estimate the ranges of Kasner parameters that characterize the conditions for the system to hit one of those quantum walls. Let us assume a trajectory that is following a Kasner dynamics with small fluctuations relatively close to the singularity. That is, α is already large enough (in absolute value) so that all the terms of the form $1/\alpha$ can be neglected in (29), but not so large yet as to make terms proportional to B_i^2/P_Q^2 relevant. In such a scenario, all the dependence on α can be neglected in the exponentials (29). If one then requires all of them to be nonnegative, so that none of the potential terms is growing along evolution, the

following three ranges of values are obtained,

$$\begin{aligned}
p_- \geq 0 \quad \text{and} \quad \frac{1}{4} (\sqrt{9-3r} - \sqrt{1+r}) &\leq \frac{p_+}{(p_+^2 + p_-^2)^{1/2}} \leq \frac{1}{2} \sqrt{1+r}, \\
p_- < 0 \quad \text{and} \quad \frac{1}{4} (\sqrt{9-3r} - \sqrt{1+r}) &\leq \frac{p_+}{(p_+^2 + p_-^2)^{1/2}} \leq \frac{1}{2} \sqrt{1+r}, \\
\frac{p_+}{(p_+^2 + p_-^2)^{1/2}} &\leq -\frac{1}{4} (\sqrt{9-3r} + \sqrt{1+r}),
\end{aligned} \tag{30}$$

where $r := (B_1^2 + B_2^2)/(p_+^2 + p_-^2)$. If the parameters of the system lie in any of these ranges, the system will follow its Kasner dynamics without hitting any classical potential wall until the fluctuations B_i^2/P_Q^2 become dominant. This is when the system bounces against a quantum wall. Note that in the classical limit $r \rightarrow 0$, the above ranges correspond to the classical exits, $\{p_- < 0, p_+ = -\frac{p_-}{\sqrt{3}}\}$, $\{p_- > 0, p_+ = \frac{p_-}{\sqrt{3}}\}$, and $\{p_- = 0, p_+ \leq 0\}$, respectively.

Intuitively the above relations define three wedges on the plane of anisotropies. The classical convex potential walls depicted in Fig. 1 are pushed back from the three symmetry axes by the quantum effects creating such wedges. These wedges do not reach infinity, though, as they are closed by the new quantum potential walls produced by the fluctuations B_i^2/P_Q^2 . Therefore, these quantum contributions form concave caps connecting classical walls, and constraining the dynamics of the system to a finite region of the phase space.

5 Analysis of the chaos

As explained in the introduction, the classical Mixmaster model shows a chaotic behavior close to the singularity. In the context of general relativity, and specifically for the Mixmaster model, two methods have been proposed in the literature to study the chaotic nature of this system without ambiguities. The first one makes use of the covariantly defined Lyapunov exponent [19, 52], while the second one is based on the study of the fractal structure of the space of initial conditions [21]. In the following, both methods will be applied to our semiclassical system in order to check how quantum fluctuations modify the classical results. More precisely, in Sec. 5.1 we will present a canonical transformation to a set of variables that generalize the Misner-Chitre variables, which will allow us to compute the Lyapunov exponent, and construct an isomorphism between the quantum Mixmaster dynamics and the geodesic flow on a four-dimensional curved manifold. The conclusion of this method will be that the quantum dynamics is still chaotic. In Sec. 5.2 we will be able to provide a quantitative measure of the chaos by making use of the fractal method, and will show that, as compared to the classical system, the quantum system has a reduced degree of chaos.

5.1 Covariant Lyapunov exponent

The Lyapunov exponent is an accurate way of representing chaos in dynamical systems as long as the following conditions are satisfied [18]:

1. The system is autonomous.
2. The relevant part of the phase space is bounded.
3. The invariant measure is normalizable.
4. The domain of the time parameter is infinite.

The classical dynamics of the Mixmaster model described by the shape parameters β_{\pm} and their conjugate momenta p_{\pm} in terms of the internal time α does not obey all of the above conditions. Namely, while the domain of the time parameter α is infinite, the system (8)–(11) is not autonomous due to the explicit term $e^{4\alpha}$. Moreover, due to the appearance of this same factor in the Hamiltonian (7), asymptotically the height of the potential walls is effectively diminished making the accessible region of the phase space unbounded. However, for the classical model one can perform a canonical transformation to a new set of variables introduced by Misner and Chitre [19, 53], which defines an asymptotically time-independent potential term in the Hamiltonian. In terms of these variables the potential walls are stationary, defining a bounded region of the phase

space for the dynamics of the system, and can be approximated by infinite potential walls fixed at certain positions. Furthermore, the dynamics is shown to be isomorphic to the geodesic flow of a curved two-dimensional Riemannian manifold. This picture is very helpful and allows, in particular, to compute the corresponding Lyapunov exponent by analyzing the geodesic deviation equation on that manifold.

Here, we will generalize the classical analysis by constructing a canonical transformation for our quantum system (21)–(24), which will lead to a new set of variables that obey the properties detailed above. Furthermore, an isomorphism to the geodesic motion on a four-dimensional Riemannian manifold will be obtained, and the corresponding Lyapunov exponent will be computed.

5.1.1 Generalized Misner-Chitre variables

Let us start by implicitly defining the generalized Misner-Chitre variables $(\Gamma, \xi, \theta, \sigma, \phi)$ by the following transformation,

$$\begin{aligned}\alpha &= -e^\Gamma \xi, \\ \beta_+ &= e^\Gamma \sqrt{\xi^2 - 1} \cos \theta, \\ \beta_- &= e^\Gamma \sqrt{\xi^2 - 1} \sin \theta \cos \sigma, \\ s_1 &= e^\Gamma \sqrt{\xi^2 - 1} \sin \theta \sin \sigma f_+(\phi, p_\phi), \\ s_2 &= e^\Gamma \sqrt{\xi^2 - 1} \sin \theta \sin \sigma f_-(\phi, p_\phi),\end{aligned}\tag{31}$$

for configuration variables, and their conjugate momenta $(p_\Gamma, p_\xi, p_\theta, p_\sigma, p_\phi)$ by the relations

$$\begin{aligned}p_\alpha &= e^{-\Gamma} [(\xi^2 - 1)p_\xi - \xi p_\Gamma], \\ p_+ &= e^{-\Gamma} \left[\cos \theta \sqrt{\xi^2 - 1} (\xi p_\xi - p_\Gamma) - \frac{\sin \theta}{\sqrt{\xi^2 - 1}} p_\theta \right], \\ p_- &= e^{-\Gamma} \left[\sin \theta \cos \sigma \sqrt{\xi^2 - 1} (\xi p_\xi - p_\Gamma) + \frac{\cos \theta \cos \sigma}{\sqrt{\xi^2 - 1}} p_\theta - \frac{\csc \theta \sin \sigma}{\sqrt{\xi^2 - 1}} p_\sigma \right], \\ p_{s_1} &= e^{-\Gamma} f_+(\phi, p_\phi) \left[\sin \sigma \sin \theta \sqrt{\xi^2 - 1} (\xi p_\xi - p_\Gamma) + \frac{\cos \theta}{\sqrt{\xi^2 - 1}} p_\theta + \frac{\csc \theta \cos \sigma}{\sqrt{\xi^2 - 1}} p_\sigma - \frac{h(p_\phi) \csc \theta \csc \sigma \cos 2\phi}{2p_\phi f_+^2(\phi, p_\phi) \sqrt{\xi^2 - 1}} \right], \\ p_{s_2} &= e^{-\Gamma} f_-(\phi, p_\phi) \left[\sin \theta \sin \sigma \sqrt{\xi^2 - 1} (\xi p_\xi - p_\Gamma) + \frac{\cos \theta \sin \sigma}{\sqrt{\xi^2 - 1}} p_\theta + \frac{\csc \theta \cos \sigma}{\sqrt{\xi^2 - 1}} p_\sigma + \frac{h(p_\phi) \csc \theta \csc \sigma \cos 2\phi}{2p_\phi f_-^2(\phi, p_\phi) \sqrt{\xi^2 - 1}} \right],\end{aligned}\tag{32}$$

where the functions $f_+(\phi, p_\phi)$, $f_-(\phi, p_\phi)$, and $h(p_\phi)$ are defined as follows,

$$f_+(\phi, p_\phi) := \frac{1}{\sqrt{2}|p_\phi|} (p_\phi^2 + U_1 - U_2 - h(p_\phi) \sin 2\phi)^{1/2},\tag{33}$$

$$f_-(\phi, p_\phi) := \frac{1}{\sqrt{2}|p_\phi|} (p_\phi^2 - U_1 + U_2 + h(p_\phi) \sin 2\phi)^{1/2},\tag{34}$$

$$h(p_\phi) := \sqrt{(p_\phi^2 - (U_1 + U_2))^2 - 4U_1U_2}.\tag{35}$$

The domain of definition of the different variables is given by $\theta, \sigma \in (0, \pi)$, $\xi \geq 1$, $p_\xi, p_\theta, p_\sigma, p_\Gamma, \Gamma \in \mathbb{R}$, while the pair (ϕ, p_ϕ) takes values in the ranges $\phi \in [0, 2\pi)$, and $p_\phi \in \mathbb{R}$ is restricted under the condition that the above functions f_+ , f_- , and h are real. For the classical system, only the variables (Γ, ξ, θ) are defined, along with their corresponding conjugate momenta $(p_\Gamma, p_\xi, p_\theta)$. In order to encode the quantum degrees of freedom, the new angular variables (σ, ϕ) and their momenta (p_σ, p_ϕ) have been introduced. The classical configuration space corresponds to the union of the two half-planes $\sigma \rightarrow 0$ and $\sigma \rightarrow \pi$. Note that points in this plane are unreachable for the quantum system since s_1 and s_2 would be vanishing there, violating the uncertainty principle. This does not only apply to the classical plane, but also to other sets of points such as those given by $\sin \theta = 0$, $f_+(\phi, p_\phi) = 0$, or $f_-(\phi, p_\phi) = 0$.

This canonical transformation is parameterized by the constants of motion U_1 and U_2 , which encode information about the saturation of the uncertainty relation. If U_1 and U_2 could be ignored, the functions (33)–(35)

would simplify to $f_+ = |\cos(\phi + \pi/4)|$, $f_- = |\sin(\phi + \pi/4)|$, and $h = p_\phi^2$. The configuration space mapping (31) would then be a direct generalization of 2-dimensional polar coordinates on the classical anisotropy plane to a 4-dimensional quantum version. Inclusion of the U -terms requires a deformation of the 3-sphere mapping according to (33)–(34). The functions f_+ and f_- are then nonzero because U_1 and U_2 are positive, and so are s_1 and s_2 due to the restrictions of θ and σ to the range $(0, \pi)$. Note also that the condition that $h(p_\phi)$ be real imposes a lower bound on $|p_\phi|$ for nonzero U_1 and U_2 . The original repulsive terms U_1/s_1^2 and U_2/s_2^2 in the effective potential are now replaced by a lower bound on the angular momentum in the s_1 - s_2 plane.

If we now choose Γ as the internal time variable, the Hamiltonian that governs the dynamics of the remaining variables $(\xi, \theta, \sigma, \phi)$ with respect to Γ is given by

$$\mathcal{H} = \left[p_\xi^2(\xi^2 - 1) + \frac{p_\theta^2}{\xi^2 - 1} + \frac{p_\sigma^2}{(\xi^2 - 1)\sin^2 \theta} + \frac{p_\phi^2}{(\xi^2 - 1)\sin^2 \theta \sin^2 \sigma} + 2e^{2\Gamma - 4\xi e^\Gamma} V_Q \right]^{1/2}. \quad (36)$$

The potential term is obtained by simply applying the above canonical transformation to its definition (20), and its full contribution to the Hamiltonian can be written as a linear combination of exponential terms,

$$2e^{2\Gamma - 4\xi e^\Gamma} V_Q = \frac{e^{2\Gamma}}{3} \left(e^{-4\xi e^\Gamma E_1} + e^{-4\xi e^\Gamma E_2} + e^{-4\xi e^\Gamma E_3} \right) - \frac{2}{3} e^{2\Gamma} \left(e^{-4\xi e^\Gamma E_4} + e^{-4\xi e^\Gamma E_5} + e^{-4\xi e^\Gamma E_6} \right), \quad (37)$$

with the same exponents $\{E_i\}_{i=1}^6$ defined above (26). In terms of the new variables, these exponents take the explicit form

$$\begin{aligned} E_1 &= 1 + \frac{2\sqrt{\xi^2 - 1}}{\xi} \cos \theta - \frac{8e^\Gamma(\xi^2 - 1)}{\xi} \sin^2 \theta \sin^2 \sigma f_+^2(\phi, p_\phi), \\ E_2 &= 1 - \frac{\sqrt{\xi^2 - 1}}{\xi} (\cos \theta + \sqrt{3} \sin \theta \cos \sigma) - \frac{2e^\Gamma(\xi^2 - 1)}{\xi} \sin^2 \theta \sin^2 \sigma [f_+^2(\phi, p_\phi) + 3f_-^2(\phi, p_\phi)], \\ E_3 &= 1 - \frac{\sqrt{\xi^2 - 1}}{\xi} (\cos \theta - \sqrt{3} \sin \theta \cos \sigma) - \frac{2e^\Gamma(\xi^2 - 1)}{\xi} \sin^2 \theta \sin^2 \sigma [f_+^2(\phi, p_\phi) + 3f_-^2(\phi, p_\phi)], \\ E_4 &= 1 - \frac{\sqrt{\xi^2 - 1}}{\xi} \cos \theta - \frac{2e^\Gamma(\xi^2 - 1)}{\xi} \sin^2 \theta \sin^2 \sigma f_+^2(\phi, p_\phi), \\ E_5 &= 1 + \frac{\sqrt{\xi^2 - 1}}{2\xi} (\cos \theta - \sqrt{3} \sin \theta \cos \sigma) - \frac{e^\Gamma(\xi^2 - 1)}{2\xi} \sin^2 \theta \sin^2 \sigma [f_+^2(\phi, p_\phi) + 3f_-^2(\phi, p_\phi)], \\ E_6 &= 1 + \frac{\sqrt{\xi^2 - 1}}{2\xi} (\cos \theta + \sqrt{3} \sin \theta \cos \sigma) - \frac{e^\Gamma(\xi^2 - 1)}{2\xi} \sin^2 \theta \sin^2 \sigma [f_+^2(\phi, p_\phi) + 3f_-^2(\phi, p_\phi)]. \end{aligned} \quad (38)$$

The singularity is now located at $\Gamma \rightarrow \infty$, which ensures the fulfillment of condition 4 above, and thus the potential (37) will be asymptotically negligible as long as all exponential terms (38) are positive. In the classical case, which can be recovered simply by imposing $\sin \sigma \rightarrow 0$ in (38), all these exponents turn out to be independent of Γ . Therefore, Π , defined as the region of the configuration space where the potential is negligible, can be shown to be compact and time independent. Outside this region, the potential will tend to infinity and the system will be prevented from being located there. In this way, the potential can be asymptotically approximated by certain combination of stationary walls and condition 2 above is met.

Quantum contributions, however, render the above exponents E_i time dependent. Therefore, the shape of the region Π will also change with Γ . The key issue to check is whether such a dependence could make the region Π noncompact and spoil the good properties of the classical Misner-Chitre variables. The answer, though, is in the negative. As can be easily checked in the explicit expression of the exponents (38), all quantum terms have a negative contribution, so their relevance increases as the singularity is approached. Thus, as Γ tends to infinity, quantum contributions decrease the value of every exponent E_i and, in this way, make the region Π shrink. In fact, except in the planes defined by the values $\sin \sigma \rightarrow 0$ and $\sin \theta \rightarrow 0$, from certain value of Γ on, the relevance of the quantum effects will be such that all the exponents E_i will be negative. Therefore, outside the mentioned planes, the potential term will not be negligible anywhere and the region Π will be restricted to the sets of points defined by $\sin \theta \rightarrow 0$ and $\sin \sigma \rightarrow 0$, which are forbidden for the quantum system. This is related to the closed-off classical exits mentioned above: while in the classical system there are certain values of the parameters which avoid the potential all along until the singularity, in the quantum system any value of the parameters will lead, sooner or later, to an interaction with the potential.

In the strict limit of $\Gamma \rightarrow \infty$ the region Π is empty, but any finite range of large values of Γ implies a nonempty and bounded set. In any such region, independently of the specific finite range of Γ , the Hamiltonian in terms of the generalized Misner-Chitre variables is given by just the kinetic terms, namely,

$$\mathcal{H} = \left[p_\xi^2 (\xi^2 - 1) + \frac{p_\theta^2}{\xi^2 - 1} + \frac{p_\sigma^2}{(\xi^2 - 1) \sin^2 \theta} + \frac{p_\phi^2}{(\xi^2 - 1) \sin^2 \theta \sin^2 \sigma} \right]^{1/2}. \quad (39)$$

Since it does not depend explicitly on time, it is constant under evolution and defines the conserved energy of the dynamical system $E = \mathcal{H}$. Consequently, the system of equations of motion (21)–(24) written for the new variables becomes autonomous, and condition 1 above is fulfilled.

As we already showed, by introducing our new set of variables, we have been able to restrict the relevant part of the phase space to a bounded region Π , and thus condition 2 of the above criteria is satisfied. Moreover, in this same region and asymptotically, following the same rationale as in the classical case [52], one can conclude that the invariant measure is normalizable, satisfying thus also condition 3. Finally, following condition 4, the domain of the time parameter Γ is infinite, all conditions 1–4 listed above are met. The sign of the Lyapunov exponent that can be computed for these variables is thus invariant, and will characterize the possible chaos of the system.

5.1.2 Isomorphism to a geodesic flow on a Riemannian manifold

In order to compute the Lyapunov exponent, it is very useful to note that the above Hamiltonian (39) has a form similar to the Hamiltonian $(\frac{1}{2} g_{\mu\nu} p^\mu p^\nu)^{1/2}$ of a free particle evolving on a curved background with metric $g_{\mu\nu}$. Therefore, asymptotically (for any finite range of large values of Γ , as explained in the preceding subsection), the Mixmaster dynamics inside the exponential walls is isomorphic to the geodesic flow on the 4-dimensional Riemannian manifold with metric

$$g_{\mu\nu} dx^\mu dx^\nu = E^2 \left[\frac{d\xi^2}{\xi^2 - 1} + (\xi^2 - 1) d\theta^2 + (\xi^2 - 1) \sin^2 \theta d\sigma^2 + (\xi^2 - 1) \sin^2 \theta \sin^2 \sigma d\phi^2 \right]. \quad (40)$$

[The coordinate transformation $\xi = \cosh \psi$ shows that this space is a submanifold of a hyperboloid $|\vec{x}|^2 - t^2 = E^2$ in 5-dimensional Minkowski space-time with line element $ds^2 = E^2 (d\psi^2 + \sinh^2 \psi (d\theta^2 + \sin^2 \theta (d\sigma^2 + \sin^2 \sigma d\phi^2)))$.] This metric is maximally symmetric, with curvature scalar $R = -12/E^2$, and thus its Riemann tensor can be written as

$$R_{\tau\rho\sigma}{}^\mu = \frac{R}{12} (g_{\tau\sigma} g_\rho^\mu - g_{\rho\sigma} g_\tau^\mu) = -\frac{1}{E^2} (g_{\tau\sigma} g_\rho^\mu - g_{\rho\sigma} g_\tau^\mu). \quad (41)$$

Moreover, from this expression, it is easy to compute the sectional curvature of the manifold. That is, given any two linearly independent vector fields a^μ and b^μ , we have

$$\frac{R_{\tau\rho\sigma\nu} a^\tau b^\rho a^\sigma b^\nu}{(a^\mu a_\mu)(b^\alpha b_\alpha) - (a^\mu b_\mu)^2} = -\frac{1}{E^2}. \quad (42)$$

Therefore, the sectional curvature is constant and negative.

In order to obtain the invariant Lyapunov exponent of the system, one needs to analyze the geodesic deviation on this manifold. For such a purpose, it is very convenient to introduce the Fermi orthonormal basis,

$$\begin{aligned} e_1^\mu &= \left(\frac{\sqrt{\xi^2 - 1}}{E} \cos \gamma_1(s), \frac{\sin \gamma_1(s) \cos \gamma_2(s)}{E \sqrt{\xi^2 - 1}}, \frac{\sin \gamma_1(s) \sin \gamma_2(s) \cos \gamma_3(s)}{E \sqrt{\xi^2 - 1} \sin \theta}, \frac{\sin \gamma_1(s) \sin \gamma_2(s) \sin \gamma_3(s)}{E \sqrt{\xi^2 - 1} \sin \theta \sin \sigma} \right), \\ e_2^\mu &= \left(-\frac{\sqrt{\xi^2 - 1}}{E} \sin \gamma_1(s), \frac{\cos \gamma_1(s) \cos \gamma_2(s)}{E \sqrt{\xi^2 - 1}}, \frac{\cos \gamma_1(s) \sin \gamma_2(s) \cos \gamma_3(s)}{E \sqrt{\xi^2 - 1} \sin \theta}, \frac{\cos \gamma_1(s) \sin \gamma_2(s) \sin \gamma_3(s)}{E \sqrt{\xi^2 - 1} \sin \theta \sin \sigma} \right), \\ e_3^\mu &= \left(0, -\frac{\sin \gamma_2(s)}{E \sqrt{\xi^2 - 1}}, \frac{\cos \gamma_2(s) \cos \gamma_3(s)}{E \sqrt{\xi^2 - 1} \sin \theta}, \frac{\cos \gamma_2(s) \sin \gamma_3(s)}{E \sqrt{\xi^2 - 1} \sin \theta \sin \sigma} \right), \\ e_4^\mu &= \left(0, 0, -\frac{\sin \gamma_3(s)}{E \sqrt{\xi^2 - 1} \sin \theta}, \frac{\cos \gamma_3(s)}{E \sqrt{\xi^2 - 1} \sin \theta \sin \sigma} \right), \end{aligned} \quad (43)$$

so that $g_{\mu\nu}e_i^\mu e_j^\nu = \delta_{ij}$, where $\gamma_1, \gamma_2, \gamma_3 \in [0, 2\pi)$ are angular variables that depend on the curvilinear coordinate s . These variables are then fixed by requiring the first vector $e_1^\mu = (d\xi/ds, d\theta/ds, d\sigma/ds, d\phi/ds)$ to be tangent to the geodesics,

$$\frac{De_1^\mu}{ds} := \frac{de_1^\mu}{ds} + \Gamma^\mu_{\nu\rho}e_1^\nu e_1^\rho = 0, \quad (44)$$

where $\Gamma^\mu_{\nu\rho}$ are the Christoffel symbols of the metric (40), which leads to the equations

$$\begin{aligned} \frac{d\gamma_1(s)}{ds} &= -\frac{\xi(s) \sin \gamma_1(s)}{E\sqrt{\xi(s)^2 - 1}}, \\ \frac{d\gamma_2(s)}{ds} &= -\frac{\sin \gamma_1(s) \sin \gamma_2(s)}{E\sqrt{\xi(s)^2 - 1} \tan \theta(s)}, \\ \frac{d\gamma_3(s)}{ds} &= -\frac{\sin \gamma_1(s) \sin \gamma_2(s) \sin \gamma_3(s)}{E\sqrt{\xi(s)^2 - 1} \tan \sigma(s) \sin \theta(s)}. \end{aligned} \quad (45)$$

The basis above is constructed so that all the vectors are parallel transported along this curve and, thus,

$$\frac{De_i^\mu}{ds} = \frac{de_i^\mu}{ds} + \Gamma^\mu_{\nu\rho}e_i^\nu e_i^\rho = 0 \quad (46)$$

is obeyed for all $i = 1, 2, 3, 4$.

Let us now consider the vector Z^μ that connects two nearby geodesic curves, and obeys the geodesic deviation equation,

$$\frac{D^2 Z^\mu}{ds^2} = R_{\tau\rho\sigma}{}^\mu e_1^\sigma e_1^\rho Z^\tau, \quad (47)$$

with $R_{\tau\rho\sigma}{}^\mu$ being the Riemann tensor (41). Decomposing this vector in the above basis,

$$Z^\mu = Z_i \delta^{ik} e_k^\mu, \quad (48)$$

with $Z_i \in \mathbb{R}$, and taking into account the properties of the basis vectors e_i^μ , the geodesic deviation equation takes the form

$$\frac{d^2 Z_1}{ds^2} e_1^\mu + \frac{d^2 Z_2}{ds^2} e_2^\mu + \frac{d^2 Z_3}{ds^2} e_3^\mu + \frac{d^2 Z_4}{ds^2} e_4^\mu = \frac{1}{E^2} (Z_2 e_2^\mu + Z_3 e_3^\mu + Z_4 e_4^\mu). \quad (49)$$

Since these basis vectors are linearly independent, their coefficients on both sides of the equation must be identical, that is,

$$\frac{d^2 Z_1}{ds^2} = 0, \quad \frac{d^2 Z_2}{ds^2} = \frac{Z_2}{E^2}, \quad \frac{d^2 Z_3}{ds^2} = \frac{Z_3}{E^2}, \quad \frac{d^2 Z_4}{ds^2} = \frac{Z_4}{E^2}. \quad (50)$$

It is straightforward to obtain the solutions to these equations,

$$Z_1 = C_1 s + D_1, \quad Z_2 = C_2 e^{s/E} + D_2 e^{-s/E}, \quad Z_3 = C_3 e^{s/E} + D_3 e^{-s/E}, \quad Z_4 = C_4 e^{s/E} + D_4 e^{-s/E}, \quad (51)$$

with integration constants C_i and D_i for $i = 1, 2, 3, 4$. Then, according to [19], the invariant Lyapunov exponent of this system is given as

$$\lambda = \sup_{i=1,2,3,4} \left\{ \lim_{s \rightarrow \infty} \frac{\ln [Z_i^2 + (dZ_i/ds)^2]}{2s} \right\}. \quad (52)$$

Substituting the above solutions (51) in this definition, the invariant Lyapunov exponent is found to be

$$\lambda = \frac{1}{E}, \quad (53)$$

which is strictly positive.

As already explained, since all the conditions 1-4 detailed above are satisfied by this system, the positive value of this Lyapunov exponent (53) implies that the dynamics under consideration is chaotic. Since this geodesic flow is isomorphic to the quantum dynamics of the Mixmaster model, we can also confirm that the latter is chaotic.

5.2 The fractal dimension of the repeller

If a dynamical system has a finite number of exits or possible final outcomes (for instance, in the presence of an attractor), the space of initial conditions can be divided into different regions according to the final state of each point. The boundary between these regions can be either smooth or fractal, and the latter, as will be shown below, is a clear indicator of chaos. Given the dimension of the boundary D_0 , and the dimension of the space of initial data D , we define its difference as

$$\delta := D - D_0. \quad (54)$$

When the boundary is smooth, we have $\delta = 1$, while for a fractal structure, δ is in the range $0 < \delta < 1$. This quantity is known as the uncertainty exponent, since it is directly related to the fraction of the space of initial data with uncertain outcome [21, 54]. Specifically,

$$f(\varepsilon) \sim \varepsilon^\delta, \quad (55)$$

where ε is the error of the initial conditions, and $f(\varepsilon)$ is the fraction of uncertain outcomes in the space of initial data. Here, a point is classified as being of uncertain outcome for an error ε if, taking a hypersphere of radius ε centered around that point, it contains points with different outcomes. Nonchaotic systems do not present an amplification of the initial uncertainties, and, correspondingly, they show a linear relation between $f(\varepsilon)$ and ε . Therefore, according to (55), $\delta = 1$, which, in turn, implies that the boundary between the different regions is smooth. Chaotic systems, on the contrary, show an amplification of the initial error, which means that $0 < \delta < 1$, and that the boundaries are fractal. The lower the value of δ (and thus higher the value of D_0), the more chaotic the system is [21].

Concerning the analysis of theories with time-reparameterization invariance, like general relativity, the advantage of measuring the chaos in this way, as opposed to other dynamical techniques, is that δ is invariant. Indeed, a reparameterization of the time variable will not change the classification—in terms of different outcomes—of each point on the space of initial conditions. An initial point that has a given outcome will maintain the very same outcome under a time reparameterization, and only reach it earlier or later in the new time coordinate. Therefore, since δ is a measurable quantity, it can be used to compare the level of chaos between different systems, and this is certainly an appropriate method to study how quantum effects modify the chaotic behavior of the classical Mixmaster model.

5.2.1 Application to the Mixmaster model and numerical setup

The first step in order to apply this framework to our model, and compute the uncertainty exponent δ , is thus to define the exits or final outcomes of the system, which will divide the space of initial conditions into different regions. For the classical system, the three natural outcomes are given by the three exit trajectories. Any initial point will end up in one of these three exits, except those that follow an infinite sequence of bounces against the potential walls and form the repeller set. As explained in Sec. 4, those classical exits are closed up by quantum fluctuations. Nonetheless, our numerical simulations show that, since the fluctuations B_i/P_Q^2 are very small, the system takes a very long time to reach those quantum walls, and therefore, in practice, we can define the three ranges of values (30) as the final outcomes of our quantum system. In fact, due to the numerical nature of the analysis, it is necessary to allow an artificial extension of the ranges that define the exits. Something similar happens under the classical evolution: since a typical initial point takes a very long time to reach one of the exits, numerically one can never exactly state that a given exit has been reached. Therefore, in order to facilitate the process of escaping and reaching the outcomes, as done in the classical analysis presented in Ref. [21], a small error for the exit conditions will be allowed, as we will explain later.

Let us now parameterize the initial values of the variables $(\beta_+, \beta_-, p_+, p_-)$ as follows,

$$\begin{aligned} \beta_+|_{\alpha=\alpha_{\text{ini}}} &= \frac{1 - 2v_0(1 + u_0)}{2(1 + v_0 + u_0v_0)}\alpha_0, & \beta_-|_{\alpha=\alpha_{\text{ini}}} &= -\frac{\alpha_0\sqrt{3}}{2(1 + v_0 + u_0v_0)}, \\ p_+|_{\alpha=\alpha_{\text{ini}}} &= \frac{\omega_0}{\sqrt{6\pi}} \frac{1 - 2u_0(1 + u_0)}{1 + u_0 + u_0^2}, & p_-|_{\alpha=\alpha_{\text{ini}}} &= \frac{\omega_0}{\sqrt{2\pi}} \frac{1 + 2u_0}{1 + u_0 + u_0^2}, \end{aligned} \quad (56)$$

with the four real parameters α_0 , ω_0 , u_0 , and v_0 . In order to explore the boundaries between regions with a different outcome in the full space of initial data, already for the classical system, one would need to perform

an enormous amount of numerical simulations. Therefore, as done in Ref. [21], we will reduce our study to the cross-section (u_0, v_0) of that space, by choosing a fixed value of all the initial variables except for u_0 and v_0 . Furthermore, to compare more efficiently our results with Ref. [21], we will consider the same set of initial conditions for the expectation values as those considered in that reference for the corresponding classical variables. More precisely, ω_0 will be fixed to $\omega_0 = \frac{1}{3}$, while $\alpha_0 = \alpha_{\text{ini}}$ will be the initial time, and its value will be such that the following equation is obeyed,

$$\omega_0 = \sqrt{\frac{3\pi}{2}} H_Q|_{\alpha=\alpha_0}, \quad (57)$$

with the Hamiltonian H_Q (19), which depends on the initial value of the quantum fluctuations that will be detailed below. Finally, for the numerical analysis, a 300×300 grid in the region defined by $u_0 \in [1.34, 1.36]$ and $v_0 \in [1.3, 1.32]$ will be chosen.

Concerning the initial conditions for the quantum variables $(s_1, s_2, p_{s_1}, p_{s_2}, U_1, U_2)$, instead of choosing a fixed value for them, and in order to analyze the dimensionality of the boundaries between regions for different cross-sections of the space of initial data, we will run a number of numerical evolutions with different sets of values. In this way, we will be able to check how quantum effects modify the commented cross-section (u_0, v_0) of the space of initial data, and compute the corresponding value of δ . In order to fix the precise sets of values in a physically sensible way, the initial quantum degrees of freedom will be parameterized in terms of the Planck constant \hbar and the three numbers k , m , and n of the order of the unity, as follows,

$$\begin{aligned} s_1|_{\alpha=\alpha_0} &= s_2|_{\alpha=\alpha_0} = \sqrt{\frac{k\hbar}{2}}, \\ p_{s_1}|_{\alpha=\alpha_0} &= p_{s_2}|_{\alpha=\alpha_0} = n\sqrt{\frac{\hbar}{2k}}, \\ U_1|_{\alpha=\alpha_0} &= U_2|_{\alpha=\alpha_0} = \frac{\hbar^2}{4}(mk - n^2), \end{aligned} \quad (58)$$

with $n \in \{\pm 1, \pm 1/2, \pm 1/\sqrt{2}, 0\}$, $k \in \{0.5, 1, 1.1, 1.2, \dots, 3\}$, and $m \in \{1, 1.1, 1.2, \dots, 2, 3\}$. Among all these sets, we have chosen a sample of 160 specific values (k, m, n) , all satisfying the Heisenberg uncertainty relation (17), which, within this parameterization, reads $mk - n^2 \geq 1$.

Moreover, for the numerical simulations the value $\hbar = 10^{-6}$ has been considered for the Planck constant, and the differential equations have been discretized and evolved by making use of a fourth-order adaptive Runge-Kutta method. In particular, at each instant of the evolution, an initial time step of $d\alpha = 10^{-5}$ is considered, which is iteratively doubled until the relative error between the corresponding evolutions with a step $2d\alpha$ and $d\alpha$ exceeds $\rho = 10^{-4}$. This method allows us to perform long numerical time evolutions during the Kasner regimes, where the variables do not perform sudden changes and evolve very smoothly. A decrease of the step size usually signals the end of the Kasner regime. In fact, since the momenta p_{\pm} remain constant during this period, the numerical algorithm periodically checks whether the system is in a Kasner regime by testing if the inequalities $|\dot{p}_+| < \rho$ and $|\dot{p}_-| < \rho$ are obeyed. If these conditions are satisfied, the algorithm verifies if the system has reached (taking into account an error) one of the outcomes (30). More specifically, as mentioned above and following the procedure described in Ref. [21], we allow an error

$$\Delta_{\text{num}} \left[\frac{p_+}{(p_+^2 + p_-^2)^{1/2}} \right] = 0.2 \left| \frac{p_-}{(p_+^2 + p_-^2)^{1/2}} \right|, \quad (59)$$

for the fraction $p_+/(p_+^2 + p_-^2)^{1/2}$, which characterizes the outcomes (30)¹. Certainly, due to this approximation, some of the initial conditions that constitute the boundary—those that are supposed to never reach a certain outcome—will also escape, but only a very small percentage [21]. Therefore, introducing this error minimally changes the division of the space of initial conditions and the subsequent analysis of the uncertainty exponent.

Depending on which of the three outcomes is reached, a specific color is assigned to that initial condition: blue, red, or green. However, for some specific initial values, the system takes a very long time to reach any of them, even if the algorithm introduces an adaptive time step. Consequently, we have introduced a maximum of $2 \cdot 10^6$ iterations for each initial value. Those points will not be assigned any color and will be part of the boundaries between regions. However, in the simulations we have performed, we have checked that very few initial data reach that maximum of iterations.

¹For more information on this error, we refer the reader to App. A.

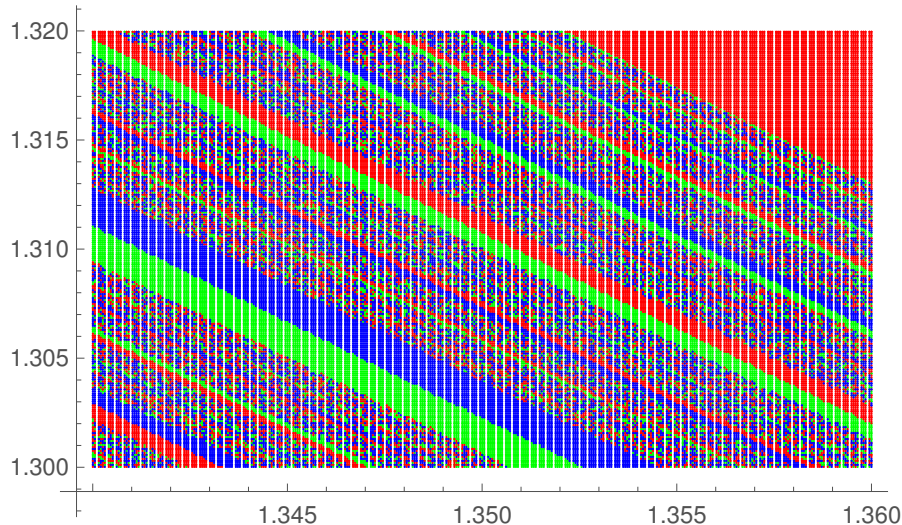


Figure 2: Division of the space of initial conditions (u_0, v_0) depending on their final outcome, considering a 300×300 grid and for the classical model.

Once the distribution of a given cross-section of the space of initial data is performed, the fraction $f(\varepsilon)$ can be computed for different values of ε (we have considered around 8–10 values for each sets of data). Finally, according to (55), simply by plotting $\ln f(\varepsilon)$ in terms of $\ln \varepsilon$ and performing a linear regression, the value of the uncertainty exponent δ can be directly obtained from the slope.

5.2.2 Results

Following the described methodology, in Ref. [21], the value $\delta = 0.14 \pm 0.01$ was obtained for the classical system. For every simulation that we have performed for different cross-sections of the space of initial data of the quantum model, a larger value has been obtained, though always $\delta < 1$. Specifically, for the sample that we have analyzed we have computed values of δ in the range $[0.42, 0.79]$. Therefore, we can conclude that, while the quantum system is still chaotic, quantum effects increase the value of the uncertainty coefficient δ , and, thus, considerably reduce its strength.

This can easily be seen, for instance, by comparing Figs. 2 and 3. In the former, the distribution of the space of initial data (u_0, v_0) is shown for the classical model, where each color (red, blue and green) represents one of the classical exits. In particular, the lack of smoothness of the boundaries conveys its fractal dimension. In the latter, on the contrary, the same space is shown for the quantum model, with certain particular initial values of the moments $(s_1, s_2, p_{s_1}, p_{s_2}, U_1, U_2)$. It is clearly visible that in this case the boundaries have been smoothed. This is just a particular example, shown for illustrative purposes, but all the cross-sections present similar behaviors, i.e., smoother distributions of the different colors in the quantum version. Furthermore, in order to show quantitatively the reduction of the level of chaos of these two particular examples, in Fig. 4 we display the linear regressions performed in the plot of $\ln f(\varepsilon)$ as a function of $\ln \varepsilon$ for each of them. In the classical case, the value $\delta = 0.14$ is recovered, while the quantum analysis leads to a larger value, $\delta = 0.51$ for this particular case.

Moreover, by comparing the simulations for different initial quantum fluctuations, we have been able to obtain some generic conclusions about the dimensionality of the boundary for different cross-sections. In particular, we have found that for initial unsqueezed states, i.e., with the same fluctuation in both conjugate variables $\Delta(\beta_{\pm}^2)|_{\alpha=\alpha_0} = \Delta(p_{\pm}^2)|_{\alpha=\alpha_0}$, the value of the correlation $\Delta(\beta_{\pm}p_{\pm})|_{\alpha=\alpha_0}$ has a different impact on the parameter δ . Namely, for states with no initial or positive correlation, $\Delta(\beta_{\pm}p_{\pm})|_{\alpha=\alpha_0} \geq 0$, the larger the value of the initial fluctuations $\Delta(\beta_{\pm}^2)|_{\alpha=\alpha_0} = \Delta(p_{\pm}^2)|_{\alpha=\alpha_0}$, the smaller the value of δ . However, states with an initial negative correlation $\Delta(\beta_{\pm}p_{\pm})|_{\alpha=\alpha_0} < 0$ show the opposite behavior: larger values of the initial fluctuations $\Delta(\beta_{\pm}^2)|_{\alpha=\alpha_0} = \Delta(p_{\pm}^2)|_{\alpha=\alpha_0}$, lead to larger values of δ . Other dependences of δ on the state properties are more complicated. For squeezed states, for instance, there is no simple pattern that describes how the sign of the initial correlation affects the value of δ as the different fluctuations increase.

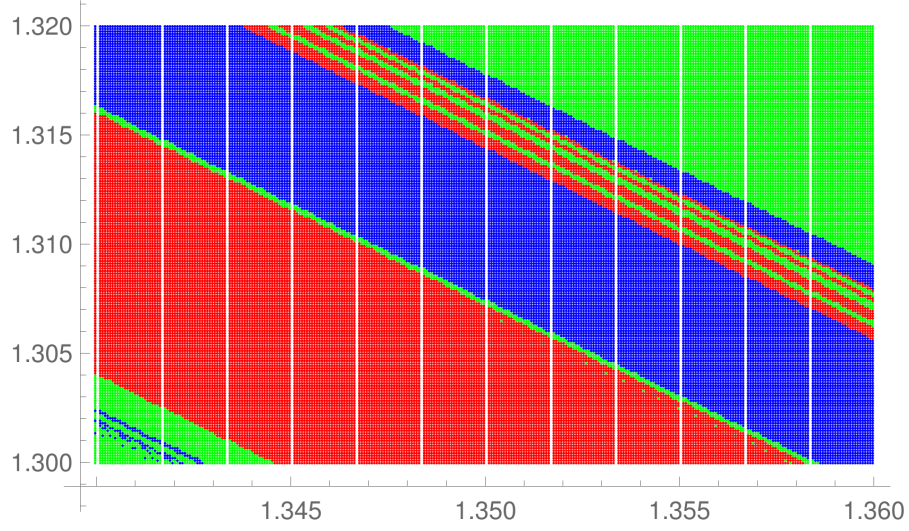


Figure 3: Division of the space of initial conditions (u_0, v_0) depending on their final outcome, considering a 300×300 grid, for the semiclassical model and with $U_1|_{\alpha=\alpha_0} = U_2|_{\alpha=\alpha_0} = \hbar^2/4$, $p_{s_1} = p_{s_2}|_{\alpha=\alpha_0} = -\sqrt{\hbar}/2$ and $s_1|_{\alpha=\alpha_0} = s_2|_{\alpha=\alpha_0} = \sqrt{\hbar}/2$.

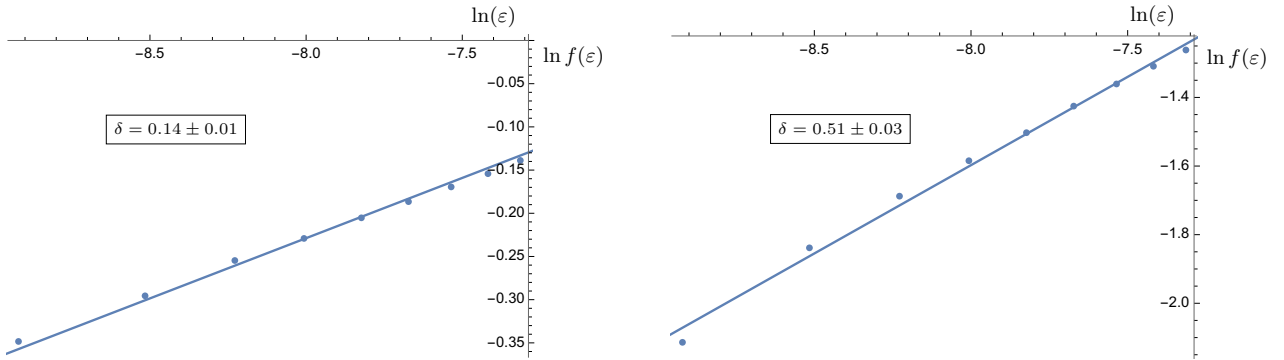


Figure 4: Linear regression of the plot $\ln f(\varepsilon)$ in terms of $\ln \varepsilon$, for the classical model (on the left) and for a quantum state (on the right) with initial $U_1|_{\alpha=\alpha_0} = U_2|_{\alpha=\alpha_0} = \hbar^2/4$, $p_{s_1}|_{\alpha=\alpha_0} = p_{s_2}|_{\alpha=\alpha_0} = -\sqrt{\hbar}/2$ and $s_1|_{\alpha=\alpha_0} = s_2|_{\alpha=\alpha_0} = \sqrt{\hbar}/2$. The value of the uncertainty exponent δ is given by the slope of the regression.

6 Conclusions

We have presented a semiclassical model that describes the vacuum Bianchi IX dynamics, in order to study how the quantum effects modify its classical chaotic behavior. The model is semiclassical as it relies on two main assumptions, namely, the relative fluctuations of the Hamiltonian are supposed to be small, while the wave function is assumed to keep a Gaussian-like shape all along evolution. We have implemented this latter condition by a suitable parameterization of higher-order moments of the evolving state. We have shown that, under such conditions, all the relevant physical information of the quantum system can be encoded in the Hamiltonian (19). In particular, the classical phase space, described by the two anisotropy variables and their momenta, is extended by another two degrees of freedom, which describe the fluctuations of the anisotropies, and two constants of motion, which contain information about the saturation of the uncertainty relations.

Concerning the quantum evolution, our numerical resolution of the equations of motion (21)–(24) has shown a similar qualitative picture as the classical dynamics. As it approaches the singularity, the system follows a succession of kinetically dominated periods, known as Kasner regimes, and quick transitions, which arise when the potential term of the Hamiltonian becomes nonnegligible. This dynamics can be understood as a particle propagating in the anisotropy plane and bouncing against the potential walls shown in Fig. 1. The main novel feature of the quantum system is the closing off of the classical exit channels. If the velocity vector of the classical particle is exactly parallel to one of the three symmetry axes of the potential, its corresponding Kasner regime lasts until the singularity is reached. For the quantum system, we have analytically shown that quantum fluctuations widen these classical exit channels, so that the velocity of the particle does not need to be exactly parallel to the symmetry axis for it to avoid the classical potential walls. However, as it evolves, new quantum terms in the potential progressively become more relevant until, eventually, they put an end to the corresponding Kasner regime in all the cases, and prevent the anisotropy parameters from reaching infinity.

Intuitively, instead of the three vertices of the classical potential shown in Fig. 1, the quantum system presents three wedges, which are closed off at a finite distance from the origin. An important consequence of this effect is that the dynamics of the system is now limited to a finite region of the configuration space. In addition, concerning the possible chaotic behavior of the system, this picture already suggests that quantum effects might decrease the level of chaos. While in the classical model all potential walls are convex, and thus defocusing, which ensures chaos, the closed-off of the classical exits necessarily implies the presence of certain concave portions of the walls.

In order to perform a more systematic study of chaos of the quantum system, we note that the present semiclassical model is formulated as a canonical system, and thus standard dynamical-systems techniques can be applied. In particular, two key methods have been implemented, which are especially well suited for systems with reparameterization invariance, such as general relativity.

First, the generalized version of the Misner-Chitre variables (31)–(32) has been constructed. In the classical set-up these variables asymptotically define stationary potential walls on the phase space, which render the dynamically accessible region compact. In the quantum case, this region is not only compact, but it also shrinks as the singularity is approached. In fact, in a strict asymptotic limit, the region is reduced to hypersurfaces in the configuration space that are inaccessible due to the uncertainty relations. Furthermore, we have also shown that the dynamics can be mapped to a geodesic motion on a curved Riemannian manifold, extending in this way the classical billiard picture. Making use of the geodesic deviation equation, we have computed the covariant Lyapunov exponent and found it to be strictly positive, which characterizes the quantum system to be chaotic.

In a second step, we have numerically computed the dimension of the boundary between regions with different outcomes in the space of initial data. More specifically, after numerically computing its evolution, each set of initial data is characterized by its final state in one of the three possible outcomes of the system, defined as the three wedges commented above. In Figs. 2 and 3 one can see a given cross-section of the space of initial data for the classical and quantum system, respectively, where each color corresponds to a given outcome. In the classical plot (Fig. 2) the fractal nature of the boundary between regions with a different outcome is clearly visible. However, in the quantum case (Fig. 3), the boundaries are smoothed out, which already signals a decrease of the level of chaos. This has been verified by numerically computing the dimension of the mentioned boundary for a large number of initial data sets. Our results are therefore robust and, in all the analyzed cases, we have found out that, even if the boundary is still fractal, its dimension is larger than that of its classical counterpart. Therefore, although the quantum system is still chaotic, quantum effects severely reduce its level.

Acknowledgments

DB and SFU thank, respectively, the Max-Planck-Institut für Gravitationsphysik and The Pennsylvania State University for hospitality while part of this work was done. SFU was funded by an FPU fellowship and a mobility scholarship of the Spanish Ministry of Universities. This work was supported in part by NSF grant PHY-2206591, the Alexander von Humboldt Foundation, the Basque Government Grant IT1628-22, and by the Grant PID2021-123226NB-I00 (funded by MCIN/AEI/10.13039/501100011033 and by “ERDF A way of making Europe”).

A Computation of the error of the outcomes

In this appendix, we provide the relation between the error that we have considered in the algorithm for the outcomes, given by (59) in terms of p_{\pm} , and the one introduced in Ref. [21], in terms of a single parameter $u \geq 1$. Following the notation of that reference, let us start by defining the so-called Kasner exponents:

$$\begin{aligned} p_1 &:= \frac{1}{3} \left[1 + \frac{p_+}{(p_+^2 + p_-^2)^{1/2}} + \frac{\sqrt{3}p_-}{(p_+^2 + p_-^2)^{1/2}} \right], \\ p_2 &:= \frac{1}{3} \left[1 + \frac{p_+}{(p_+^2 + p_-^2)^{1/2}} - \frac{\sqrt{3}p_-}{(p_+^2 + p_-^2)^{1/2}} \right], \\ p_3 &:= \frac{1}{3} \left[1 - \frac{2p_+}{(p_+^2 + p_-^2)^{1/2}} \right]. \end{aligned} \quad (60)$$

These exponents satisfy the relations $p_1 + p_2 + p_3 = p_1^2 + p_2^2 + p_3^2 = 1$, such that we can parameterize them in terms of a single parameter $u \geq 1$. Specifically, if one defines $p_{\min} := \min\{p_1, p_2, p_3\}$, $p_{\max} := \max\{p_1, p_2, p_3\}$, and $p_{\text{int}} := \{p_1, p_2, p_3\} - \{p_{\min}, p_{\max}\}$, the momenta can be parameterized as follows:

$$p_{\min} = -\frac{u}{1+u+u^2}, \quad p_{\text{int}} = \frac{1+u}{1+u+u^2}, \quad p_{\max} = \frac{u(1+u)}{1+u+u^2}. \quad (61)$$

From here, one can just compute the value of u directly,

$$u = -\frac{1+p_{\min} + \sqrt{1+2p_{\min} - 3p_{\min}^2}}{2p_{\min}}. \quad (62)$$

The classical exits, $\{p_- < 0, p_+ = -\frac{p_-}{\sqrt{3}}\}$, $\{p_- > 0, p_+ = \frac{p_-}{\sqrt{3}}\}$, and $\{p_- = 0, p_+ \leq 0\}$, correspond to $p_{\min} = 0$, as can be seen from (60). Consequently, according to (61), they are characterized by $u \rightarrow \infty$. However, if one wants to analyze numerically whether the system verifies this condition for a given time, it is not possible to obtain such precision. Therefore, in Ref. [21], they relaxed this requirement and considered $u > 8$ as a sufficient condition for the system to be in an exit. This can be interpreted as widening the exits shown in Fig. 1. Even though this approximation may seem quite extreme, only about 1% of the uncertain points escape as proved in Ref. [21], and thus the distribution of the space of initial data is minimally affected.

Then, if one wants to compute this error in terms of $p_+/(p_+^2 + p_-^2)^{1/2}$, which is the ratio we are using in our set-up to define the exits (30), one just needs to make use of the above definitions (60) and (61). First, we obtain that $u > 8$ corresponds to the intervals $p_{\min} \in (-\frac{8}{73}, 0]$, $p_{\text{int}} \in [0, \frac{9}{73})$, and $p_{\max} \in (\frac{72}{73}, 1]$ for the different momenta. Thus, we can distinguish six different cases, depending on which of the Kasner exponents p_1, p_2 , and p_3 defines p_{\min} , p_{\max} , and p_{int} :

- 1st case: $p_1 \in (-\frac{8}{73}, 0]$, $p_2 \in [0, \frac{9}{73})$, and $p_3 \in (\frac{72}{73}, 1]$,
- 2nd case: $p_1 \in (-\frac{8}{73}, 0]$, $p_2 \in (\frac{72}{73}, 1]$, and $p_3 \in [0, \frac{9}{73})$,
- 3rd case: $p_1 \in [0, \frac{9}{73})$, $p_2 \in (-\frac{8}{73}, 0]$, and $p_3 \in (\frac{72}{73}, 1]$,
- 4th case: $p_1 \in [0, \frac{9}{73})$, $p_2 \in (\frac{72}{73}, 1]$, and $p_3 \in (-\frac{8}{73}, 0]$,
- 5th case: $p_1 \in (\frac{72}{73}, 1]$, $p_2 \in [0, \frac{9}{73})$, and $p_3 \in (-\frac{8}{73}, 0]$,

- 6th case: $p_1 \in (\frac{72}{73}, 1]$, $p_2 \in (-\frac{8}{73}, 0]$, and $p_3 \in [0, \frac{9}{73})$.

If we invert the relations (60), we can write,

$$\frac{p_+}{(p_+^2 + p_-^2)^{1/2}} = \frac{1}{2}(1 - 3p_3), \quad \frac{p_-}{(p_+^2 + p_-^2)^{1/2}} = \frac{\sqrt{3}}{2}(p_1 - p_2). \quad (63)$$

Consequently, in terms of these ratios, the intervals defined in the six cases above read,

- 1st case: $\frac{p_+}{(p_+^2 + p_-^2)^{1/2}} \in [-1, -\frac{143}{146}]$ and $\frac{p_-}{(p_+^2 + p_-^2)^{1/2}} \in (-\frac{17\sqrt{3}}{146}, 0]$,
- 2nd case: $\frac{p_+}{(p_+^2 + p_-^2)^{1/2}} \in (\frac{23}{73}, \frac{1}{2}]$ and $\frac{p_-}{(p_+^2 + p_-^2)^{1/2}} \in (-\frac{40\sqrt{3}}{73}, -\frac{\sqrt{3}}{2}]$,
- 3rd case: $\frac{p_+}{(p_+^2 + p_-^2)^{1/2}} \in [-1, -\frac{143}{146}]$ and $\frac{p_-}{(p_+^2 + p_-^2)^{1/2}} \in [0, \frac{17\sqrt{3}}{146})$,
- 4th case: $\frac{p_+}{(p_+^2 + p_-^2)^{1/2}} \in [\frac{1}{2}, \frac{97}{146})$ and $\frac{p_-}{(p_+^2 + p_-^2)^{1/2}} \in [-\frac{\sqrt{3}}{2}, -\frac{63\sqrt{3}}{146})$,
- 5th case: $\frac{p_+}{(p_+^2 + p_-^2)^{1/2}} \in [\frac{1}{2}, \frac{97}{146})$ and $\frac{p_-}{(p_+^2 + p_-^2)^{1/2}} \in (\frac{63\sqrt{3}}{146}, \frac{\sqrt{3}}{2}]$,
- 6th case: $\frac{p_+}{(p_+^2 + p_-^2)^{1/2}} \in (\frac{23}{73}, \frac{1}{2}]$ and $\frac{p_-}{(p_+^2 + p_-^2)^{1/2}} \in [\frac{\sqrt{3}}{2}, \frac{40\sqrt{3}}{73})$.

As one can note, the intervals for both $\arccos[p_+/(p_+^2 + p_-^2)^{1/2}]$ and $\arcsin[p_-/(p_+^2 + p_-^2)^{1/2}]$ have the same length in all the six cases, that is,

$$\Delta_{\text{num}} \left[\arccos \left(\frac{p_+}{(p_+^2 + p_-^2)^{1/2}} \right) \right] = \Delta_{\text{num}} \left[\arcsin \left(\frac{p_-}{(p_+^2 + p_-^2)^{1/2}} \right) \right] \approx 0.2. \quad (64)$$

Finally, from here we can estimate the length of the interval for the ratio $p_+/(p_+^2 + p_-^2)^{1/2}$ defined by the condition $u > 8$, that is, its corresponding error:

$$\Delta_{\text{num}} \left[\frac{p_+}{(p_+^2 + p_-^2)^{1/2}} \right] \approx \Delta_{\text{num}} \left[\arccos \left(\frac{p_+}{(p_+^2 + p_-^2)^{1/2}} \right) \right] \left| \frac{p_-}{(p_+^2 + p_-^2)^{1/2}} \right| \approx 0.2 \left| \frac{p_-}{(p_+^2 + p_-^2)^{1/2}} \right|, \quad (65)$$

where, in the first equality, we have used that $\Delta_{\text{num}}(\arccos(x)) \approx \left| \frac{d \arccos(x)}{dx} \right| \Delta_{\text{num}} x = \frac{\Delta_{\text{num}} x}{\sqrt{1-x^2}}$.

References

- [1] V. A. Belinskii, I. M. Khalatnikov, and E. M. Lifschitz, Oscillatory approach to a singular point in the relativistic cosmology, *Adv. Phys.* **19**, 524 (1970).
- [2] C. W. Misner, Mixmaster universe, *Phys. Rev. Lett.* **22**, 1071 (1969).
- [3] C. W. Misner, Quantum Cosmology. I, *Phys. Rev.* **186**, 1319 (1969).
- [4] B. K. Berger, Numerical approaches to spacetime singularities, *Living Rev. Relativity* **5**, **1** (2002).
- [5] D. Garfinkle, Numerical simulations of generic singularities, *Phys. Rev. Lett.* **93**, 161101 (2004).
- [6] J. M. Heinzle, C. Uggla, and W. C. Lim, Spike oscillations, *Phys. Rev. D* **86**, 104049 (2012).
- [7] *Deterministic Chaos in General Relativity* eds. D Hobill, A. Burd, and A. Coley, (Plenum Press, New York, 1994).
- [8] J. D. Barrow and F. Tipler, Analysis of the generic singularity studies by Belinskii, Khalatnikov, and Lifschitz, *Phys. Rep.* **56**, 372 (1979).
- [9] J. D. Barrow, Chaos in the Einstein Equations, *Phys. Rev. Lett.* **46**, 963 (1981).
- [10] J. D. Barrow, Chaotic behaviour in general relativity, *Phys. Rep.* **85**, 1 (1982).

- [11] D. F. Chernoff and J. D. Barrow, Chaos in the Mixmaster Universe , Phys. Rev. Lett. **50**, 134 (1983).
- [12] S. E. Rugh, Cand. Scient. Thesis, The Niels Bohr Institute, (1990).
- [13] G. Francisco and G. E. A. Matsas, Qualitative and numerical study of Bianchi IX models, Gen. Rel. Grav. **20**, 1047 (1988).
- [14] B. K. Berger, Comments on the computation of Liapunov exponents for the Mixmaster universe, Gen. Rel. Grav. **23**, 1385 (1991).
- [15] D. Hobill and D. Bernstein, Classical and Quantum Gravity The Mixmaster cosmology as a dynamical system D. Simkins and M. Welge, Class. Quant. Grav. **8**, 1155 (1991).
- [16] K. Ferraz and G. Francisco, Mixmaster numerical behavior and generalizations, Phys. Rev. D **45**, 1158 (1992).
- [17] M. Szydlowski and A. Krawiec, Average rate of separation of trajectories near the singularity in mixmaster models, Phys. Rev. D **47**, 5323 (1993).
- [18] A. E. Motter, Relativistic Chaos is Coordinate Invariant, Phys. Rev. Lett. **91**, 231101 (2003).
- [19] G. P. Imponente and G. Montani, On the Covariance of the Mixmaster Chaoticity, Phys. Rev. D **63**, 103501 (2001).
- [20] Y. G. Sinai, Dynamical systems with elastic reflections, Russian Mathematical Surveys **25**, 137 (1970).
- [21] N. J. Cornish and J. J. Levin, The Mixmaster universe: A Chaotic Farey tale, Phys. Rev. D **55**, 7489 (1997).
- [22] A. E. Motter and P. S. Letelier, Mixmaster chaos, Phys. Lett. A **285**, 127 (2001).
- [23] B. K. Berger, Quantum chaos in the Mixmaster universe, Phys. Rev. D **39**, 2426 (1989).
- [24] M. Bojowald, G. Date, and G. M. Hossain, The Bianchi IX model in loop quantum cosmology, Class. Quantum Gravity **21**, 3541 (2004).
- [25] A. Kheyfets, W. A. Miller, and R. Vaulin, Quantum geometrodynamics of the Bianchi IX cosmological model, Classical Quantum Gravity **23**, 4333 (2006).
- [26] R. Benini and G. Montani, Inhomogeneous quantum Mixmaster: from classical toward quantum mechanics, Classical Quantum Gravity **24**, 387 (2007).
- [27] E. Wilson-Ewing, Loop quantum cosmology of Bianchi type IX models, Phys. Rev. D **82**, 043508 (2010).
- [28] A. Ashtekar, A. Henderson, and D. Sloan, Hamiltonian formulation of the Belinskii-Khalatnikov-Lifshitz conjecture, Phys. Rev. D **83**, 084024 (2011).
- [29] H. Bergeron, E. Czuchry, J. P. Gazeau, P. Malkiewicz, and W. Piechocki, Singularity avoidance in a quantum model of the Mixmaster universe, Phys. Rev. D **92**, 124018 (2015).
- [30] J. H. Bae, Mixmaster revisited: wormhole solutions to the Bianchi IX Wheeler–DeWitt equation using the Euclidean-signature semi-classical method, Classical Quantum Gravity **32**, 075006 (2015).
- [31] H. Bergeron, E. Czuchry, J. P. Gazeau, and P. Malkiewicz, Spectral properties of the quantum Mixmaster universe, Phys. Rev. D **96**, 043521 (2017).
- [32] E. Czuchry, D. Garfinkle, J. R. Klauder, and W. Piechocki, Do spikes persist in a quantum treatment of spacetime singularities?, Phys. Rev. D **95**, 024014 (2017).
- [33] A. Corichi and E. Montoya, Loop quantum cosmology of Bianchi IX: effective dynamics, Class. Quantum Gravity **34**, 054001 (2017).
- [34] C. Kiefer, N. Kwidzinski, and W. Piechocki, On the dynamics of the general Bianchi IX spacetime near the singularity, Eur. Phys. J. C **78**, 691 (2018).

- [35] E. Wilson-Ewing, A quantum gravity extension to the Mixmaster dynamics, *Class. Quantum Grav.* **36**, 195002 (2019).
- [36] A. Gózdź, W. Piechocki, and G. Plewa, Quantum Belinski-Khalatnikov-Lifshitz scenario, *Eur. Phys. J. C* **79**, 45 (2019).
- [37] E. Giovannetti and G. Montani, Polymer representation of the Bianchi IX cosmology in the Misner variables, *Phys. Rev. D* **100**, 104058 (2019).
- [38] D. Brizuela and S. F. Uria, Semiclassical study of the mixmaster model: The quantum Kasner map, *Phys. Rev. D* **106**, 064051 (2022).
- [39] A. Coley, No chaos in brane world cosmology, *Class. Quantum Grav.* **19**, L45 (2002).
- [40] H. Bergeron, E. Czuchry, J. P. Gazeau, P. Malkiewicz, and W. Piechocki, Smooth quantum dynamics of the Mixmaster universe, *Phys. Rev. D* **92**, 061302 (2015).
- [41] M. Bojowald, G. Date, Quantum suppression of the generic chaotic behavior close to cosmological singularities, *Phys. Rev. Lett.* **92**, 071302 (2004).
- [42] S. Antonioni and G. Montani, Singularity-free and nonchaotic inhomogeneous Mixmaster in polymer representation for the volume of the universe, *Phys. Lett. B* **790**, 475 (2019).
- [43] M. Bojowald and A. Skirzewski, Effective equations of motion for quantum system, *Rev. Math. Phys.* **18**, 713 (2006).
- [44] M. Bojowald, D. Brizuela, H. H. Hernandez, M. J. Koop, and H. A. Morales-Tecotl, High-order quantum back-reaction and quantum cosmology with a positive cosmological constant, *Phys. Rev. D* **84**, 043514 (2011).
- [45] R. Jackiw and A. Kerman, Time Dependent Variational Principle And The Effective Action, *Phys. Lett. A* **71**, 158 (1979).
- [46] F. Arickx, J. Broeckhove, W. Coene, and P. van Leuven, Gaussian Wave-packet Dynamics, *Int. J. Quant. Chem.: Quant. Chem. Symp.* **20**, 471 (1986).
- [47] O. Prezhdo, Quantized Hamiltonian Dynamics, *Theor. Chem. Acc.* **116**, 206 (2006).
- [48] T. Vachaspati and G. Zahariade, A Classical-Quantum Correspondence and Backreaction, *Phys. Rev. D* **98**, 065002 (2018).
- [49] B. Baytas, M. Bojowald, and S. Crowe, Effective potentials from semiclassical truncation, *Phys. Rev. A* **99**, 042114 (2019).
- [50] V. Belinski and M. Henneaux, *The Cosmological Singularity* (Cambridge University Press, Cambridge, England, 2017).
- [51] M. Bojowald, Canonical description of quantum dynamics, *J. Phys. A: Math. Theor.* **55**, 504006 (2022).
- [52] G. Montani et al., Classical and Quantum Features of the Mixmaster Singularity, *International Journal of Modern Physics A* **23**, 2353 (2008).
- [53] D. M. Chitre, *Investigation of Vanishing of a Horizon for Bianchi Type IX (the Mixmaster) Universe*, PhD thesis, University of Maryland (1972).
- [54] S. W. McDonald, C. Grebogi, E. Ott, and J. A. Yorke, Fractal Basin Boundaries, *Physica D: Nonlinear Phenomena* **17**, 125 (1985).